

The Impact of Ozone Production on Future Cold Point Tropopause Warming and Expansion

Stephen Bourguet

¹Harvard University, Department of Earth and Planetary Sciences, Harvard University, Cambridge, MA 02138, USA

Key Points:

- Ozone concentrations at the cold point tropopause and above 30 hPa in the tropics are approximately constant throughout the year.
- At the cold point tropopause, this concentration is determined by the origin of air and in-situ ozone production.
- Increases to the cold point tropopause height will increase local ozone production, inducing local warming and limiting further expansion.

Corresponding author: Stephen Bourguet, Stephen_Bourguet@g.harvard.edu

Abstract

A robust thermodynamic response of increased greenhouse gas forcing is an expansion of the troposphere, which may decrease ozone concentrations in the lower stratosphere and warm the tropopause. Yet, observations of lower stratospheric ozone do not agree with model projections, and the net effect of greenhouse gas forcing on the temperature structure of the region between the tropical troposphere and stratosphere is unclear. Here, I isolate the role of local ozone production in setting the height of the cold point tropopause and the ozone concentrations above this level. Increased ozone production near the tropopause following tropospheric expansion will sharpen the vertical ozone gradient of the lower stratosphere and decrease the distance between the top of the troposphere and the cold point tropopause. This would suppress tropospheric expansion and increase the water vapor concentration of the stratosphere, which amplifies global warming and contributes to stratospheric ozone destruction.

Plain Language Summary

As greenhouse gas emissions warm the earth's surface, the lowermost layer of the atmosphere will expand upwards and the middle atmosphere will cool and shrink. The effect of these changes on the ozone and temperature profiles of the region that bridges the lower and middle atmosphere has been studied previously, but there is still some debate on how these profiles will evolve. Here, I show how ozone production, which does not depend on the height of atmospheric layers, will increase within this transition region, thereby increasing its ozone concentration. This helps explain discrepancies between model projections of ozone concentrations and observations. Additionally, increased ozone concentrations will increase the temperature of air entering the stratosphere, which allows this air to hold more water vapor and has important implications for atmospheric chemistry and global warming.

1 Introduction

Tropical lower stratospheric ozone concentrations are projected to decrease following surface warming (Eyring et al., 2010), but observed decreases over the past two decades are insignificant when considering changes to tropopause height (Thompson et al., 2021). This is part of broader disagreement between ozone projections in chemistry-climate models and observations which needs to be reconciled in order to understand the recovery of the protective stratospheric ozone layer following the Montreal Protocol's global ban on halogen-containing ozone depleting substances in the late 1990s (Ball et al., 2020).

The ozone profile between the tropical tropopause and the lower stratosphere also influences atmospheric circulation and chemistry and surface climate (Ming et al., 2016). Near the tropical tropopause, ozone is a strong absorber of longwave radiation, and the temperature structure of the tropical tropopause layer (TTL) is sensitive to ozone concentrations therein (Birner & Charlesworth, 2017). This contributes to the strong static stability of the tropopause inversion layer and the lower stratosphere (Grise et al., 2010), as well as the extreme cold temperatures of the TTL which dehydrate air as it fills the stratosphere (Brewer, 1949). Water vapor impacts ozone chemistry and is a strong greenhouse gas near the tropopause (Dvortsov & Solomon, 2001; Solomon et al., 2010), and climate models project an increase in lower stratospheric water vapor with surface warming (Gettelman et al., 2010; Keeble et al., 2021). Yet, these models cannot reproduce observations, and ozone concentrations have been identified as a driver of intermodel disagreement (Gettelman et al., 2009).

The response of lower stratospheric ozone to greenhouse gas forcing is complex. Tropospheric expansion, which is a robust thermodynamic consequence of surface warming, will not simply shift the stratospheric ozone profile upwards by the extent that the tropopause

62 is displaced. Instead, the lower stratospheric ozone profile will be pushed upwards, while
63 ozone concentrations in regions dominated by photochemistry will be unaffected by the
64 transport of ozone-poor air from below (Perliski et al., 1989). In the absence of changes
65 to upwelling or production, tropopause-following coordinates would eliminate any changes
66 to lower stratospheric ozone, while an accelerated Brewer-Dobson circulation would en-
67 hance the transport of ozone-poor air into the stratosphere and decrease ozone concen-
68 trations in the region above the tropopause (Match & Gerber, 2022). On the other hand,
69 changes to the ozone production rate could increase ozone concentrations in this region
70 where the transport of ozone-poor air is balanced by local ozone production. Although
71 ozone production in the lower stratosphere is weak, it strengthens rapidly with height,
72 so the ozone concentration at the tropopause should be sensitive to its height.

73 Here, I explore how changes to ozone production following tropospheric expansion
74 above the level of zero radiative heating (LZRH) could impact ozone concentrations in
75 this region and alter the thermodynamic environment of the TTL. I do so by first es-
76 tablishing a budget for the ozone concentration at the cold point tropopause. I then con-
77 struct ozone profiles that follow from tropospheric expansion with this budget and use
78 a radiative transfer code to calculate corresponding changes to TTL temperatures and
79 water vapor concentrations. Finally, I test the robustness of this mechanism to changes
80 in tropical stratospheric upwelling.

81 **2 Data and Methods**

82 **2.1 Ozone Data**

83 Monthly-mean zonal-mean ozone profiles from the Stratospheric Water and OzOne
84 Satellite Homogenized data set (SWOOSH, Davis et al. (2016)) were used to construct
85 an ozone budget for the cold point tropopause. These data are on a pressure grid with
86 two levels near the cold point tropopause (100 hPa and 82.5 hPa), so the ozone concen-
87 trations were interpolated to the cold point tropopause height diagnosed from monthly
88 mean temperatures from the European Center for Medium-range Weather Forecasts lat-
89 est reanalysis product, ERA5 (Hersbach et al., 2020), and the Radio Occultation Me-
90 teorology Satellite Application Facility’s multi-mission data set (Ho et al., 2012; Steiner
91 et al., 2013; Gleisner et al., 2020). This was done for 2002 to 2016, which are the years
92 that all datasets were available.

93 Ozone production rates were taken from the Community Earth Systems Model’s
94 Whole Atmosphere Chemistry and Composition Model (CESM1 WACCM4). For the base
95 state, an average over 2004 to 2009 was used (data are described in Abalos et al. (2013)).
96 For two surface warming scenarios, uniform temperature increases of 3 and 5 K were im-
97 posed with CO₂ concentrations of 560 and 1000 ppm, respectively. Zonal mean ozone
98 production for each of these scenarios is shown in Figure S1.

99 **2.2 The Lagrangian Framework**

100 Ozone concentrations within the TTL balance the advection of ozone-poor air from
101 the troposphere with in-mixing of ozone-rich air from the extratropical lower stratosphere
102 and in-situ photochemical production (Abalos et al., 2013). Therefore, the Lagrangian
103 trajectory model LAGRANTO (Sprenger & Wernli, 2015) was used to trace the origin
104 of air masses that ascend to the cold point tropopause and the path they take to calcu-
105 late the cold point tropopause’s ozone budget. Following the procedure of Bourguet and
106 Linz (2022), reverse trajectories were initialized from 20°S to 20°N at all longitudes with
107 0.5° spacing on the last day of February and the last day of August in 2007, 2008, and
108 2009 near the cold point tropopause (90 hPa in boreal winter and 100 hPa in boreal sum-
109 mer). ERA5 hourly winds were used and trajectories were traced backwards for 90 days.

110 Using trajectory distributions, I construct the following budget for the cold point
111 tropopause’s ozone concentration:

$$O_{3_{c.p.}} = O_{3_{initial}} + \text{Net Production} + \text{Residual Mixing}. \quad (1)$$

112 The “initial” ozone concentration ($O_{3_{initial}}$) depends on the timescale of interest – here,
113 this is the average ozone concentration at the trajectories’ locations at the end of inte-
114 gration (90 days prior to reaching the cold point tropopause). This was calculated us-
115 ing a weighted average of SWOOSH ozone concentrations, with the weighting determined
116 by trajectory distributions. The net production term was calculated using trajectory weight-
117 ings at the end of each day, with the net ozone production field taken from WACCM’s
118 zonal mean net ozone tendency.

119 “Residual” or sub-grid scale mixing can be diagnosed with this framework by com-
120 paring the observed cold point tropopause ozone concentration to the concentration cal-
121 culated by Eq. 1 without mixing. To do so, ozone concentrations were initialized based
122 on trajectory distributions 90 days prior to reaching the cold point tropopause and then
123 increased each day according to the trajectories’ average ozone tendency. Disagreement
124 between the constructed ozone concentration at the end of the timeseries (the end of Febru-
125 ary or August) and the observed ozone concentrations were assumed to be caused by mix-
126 ing that the Lagrangian framework cannot capture. In 2007, 2008, and 2009 respectively,
127 the residual mixing terms were -3% , -8% , and -4% of the cold point tropopause’s ozone
128 concentration in February and 2% , -1% , and 14% in August. Thus, Eq. 1 can be re-
129 duced to:

$$O_{3_{c.p.}} \approx O_{3_{initial}} + \text{Net Production}. \quad (2)$$

130 **2.3 Idealized Tropospheric Expansion**

131 The following experiments are idealized representations of 3 and 5 K of surface warm-
132 ing, which would drive approximately 18 and 30 hPa of tropospheric expansion, respec-
133 tively (Match & Fueglistaler, 2021). The results shown in the text are for 5 K of warm-
134 ing; corresponding plots for 3 K are shown in the supplemental.

135 **2.3.1 Changes to Ozone at the Cold Point Tropopause**

136 To calculate how ozone concentrations at the cold point tropopause will change with
137 surface warming, it was assumed that in-mixing from the extratropics follows the tropopause
138 upwards. Anticipated increases in the meridional ozone gradient (Shepherd, 2008) and
139 mixing rates (Abalos et al., 2017) would increase the in-mixing of ozone, thereby mak-
140 ing this a conservative treatment of future in-mixing. Tropospheric ozone concentrations
141 were also assumed to remain negligible, which is reasonable given the lifetime of ozone
142 in the troposphere (Wild, 2007). These assumptions simplify the time derivative of Eq.
143 2 to:

$$\Delta O_{3_{c.p.}} = \Delta \text{Net Production}. \quad (3)$$

144 Trajectory distributions from 2008 with their pressure offset by the rate of tropo-
145 spheric expansion were used to calculate $\Delta \text{Net Production}$. This assumes that the path
146 of air en route to the cold point tropopause will follow the tropopause upwards, which
147 is consistent with the assumption of constant in-mixing from the extratropics. As dis-
148 cussed in Sections 2.1, the future zonal mean net ozone production rates are calculated
149 using WACCM.

150 **2.3.2 Temperature and Water Vapor**

151 The radiative transfer code RRTMG (Mlawer et al., 1997; Kluft et al., 2019) with
152 fixed dynamic heating was used to calculate how cold point tropopause pressures and

153 temperatures will respond to changes in the ozone profiles following tropospheric expansion.
 154 To do so, the modified ozone profile was taken from Section 4.1, and the dynamic
 155 heating profile was shifted upwards according to the rate of tropospheric expansion. Tem-
 156 peratures beneath the LZRH were increased by 3 or 5 K, and the CO₂ concentrations
 157 were increased to 560 and 1000 ppm for the two experiments, respectively. Stratospheric
 158 water vapor concentrations were calculated based on Clausius-Clapeyron relationship
 159 at the cold point tropopause at each timestep. Additional details are given in Text S1.

160 3 Observed Cold Point Tropopause Ozone Concentrations

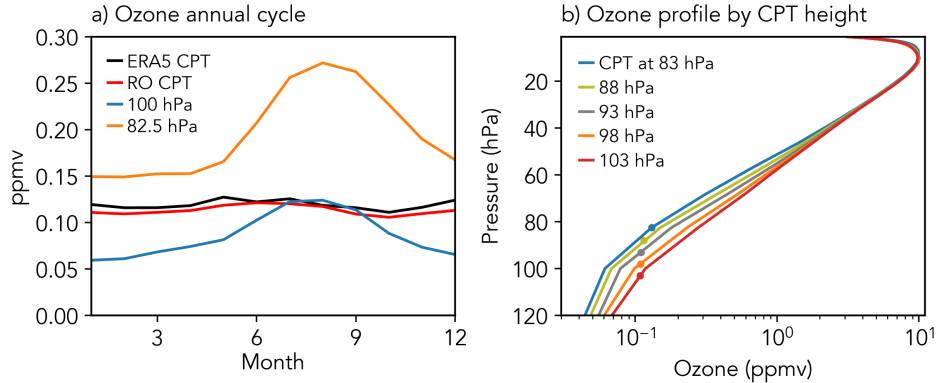


Figure 1. a) The annual cycle of zonal mean (15°S to 15°N) SWOOSH ozone concentrations at 100 hPa (blue line), 82.5 hPa (orange line), and the cold point tropopause interpolated from monthly mean radio occultations (red line) and ERA5 temperature profiles (black line). b) SWOOSH ozone profiles organized by ERA5 cold point tropopause height with the ozone concentration at the cold point tropopause marked with circles.

161 Figure 1a shows that the ozone concentration at the cold point tropopause is ap-
 162 proximately constant throughout the year, while the concentrations at nearby pressure
 163 levels vary between the solstices. In the TTL, ozone concentrations at fixed heights will
 164 vary as the transport of ozone-poor air varies (Randel et al., 2007), leading to temper-
 165 ature changes that reinforce those already driven by variations in dynamic cooling (Birner
 166 & Charlesworth, 2017). The cold point tropopause is able to follow these changes to dy-
 167 namic and radiative heating, resulting in its position on a fixed ozone surface.

168 SWOOSH ozone profiles are separated by the ERA5 cold point tropopause height
 169 in Figure 1b. These profiles emphasize the variance of lower stratospheric ozone con-
 170 centrations as the cold point tropopause moves up and down in height. Ozone concentra-
 171 tions beneath 30 hPa covary with the movement of the cold point tropopause, while con-
 172 centrations above 30 hPa are insensitive to lower stratospheric ozone variability. This
 173 reflects the division of stratospheric ozone into regimes of balanced transport and pro-
 174 duction in the lower to middle stratosphere and balanced production and loss in the mid-
 175 dle to upper stratosphere (Perliski et al., 1989). Ozone concentrations at the cold point
 176 tropopause (highlighted by circles in Figure 1b) vary by less than 0.01 ppmv as the cold
 177 point tropopause height varies by 20 hPa.

178 These observations reveal a previously overlooked feature of the cold point tropopause
 179 in the modern climate: a fixed ozone concentration of about 0.12 ppmv. Given the sea-
 180 sonal and interannual fluctuations in the height of the cold point tropopause, this fea-
 181 ture prompts the usage of cold point-relative coordinates to understand the ozone bud-
 182 get of the cold point tropopause and lowermost stratosphere.

4 Tropospheric Expansion

4.1 Ozone Profiles

To create ozone profiles that emulate the effect of 30 hPa of tropospheric expansion without increased ozone production beneath the cold point tropopause, ozone profiles were shifted up by 30 hPa and then tapered back to observations between the cold point tropopause and 30 hPa. This decreases ozone concentrations at fixed heights in the lower to middle stratosphere but does not change concentrations in tropopause-following coordinates. Ozone concentrations above 30 hPa were increased by 10% to simulate the decrease in odd-oxygen loss that would result from stratospheric cooling (Jonsson et al., 2004). (The increase aloft is not a result of tropospheric expansion but does impact TTL thermodynamics and ozone production by blocking shortwave radiation. Subsequent results are not sensitive to the choice of amplification within the range of model projections (Chiodo et al., 2018).)

To include increased ozone production between the LZRH and the cold point tropopause, the ozone concentration at the height 30 hPa above the modern cold point tropopause was calculated using Eq. 3. This would be the ozone concentration at the cold point tropopause if changes to its height were set by dynamics above the LZRH and not thermodynamics. Ozone concentrations were then increased from observations at the LZRH to this increased value at the lifted cold point tropopause.

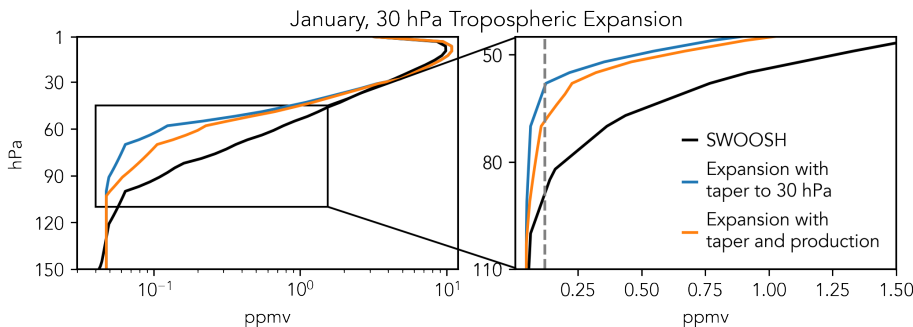


Figure 2. The 2002–2016 mean January ozone profile taken from SWOOSH (black line) and ozone profiles following 30 hPa of tropospheric expansion with and without increased ozone production (orange and blue, respectively). The 45 to 110 hPa layer is reproduced in the right panel to show the large difference near the cold point tropopause. The corresponding July ozone profile and profiles for 15 hPa of tropospheric expansion are shown in Figure S2.

The profiles for January following 30 hPa of tropospheric expansion are shown by the blue (expansion only) and orange (expansion and increased production) lines in Figure 2, with the modern ozone profile shown in black. By construction, these profiles are qualitatively similar to those in Figure 1b. In both cases, ozone varies with tropopause height in the region where transport and production are balanced, but the difference between the ozone profiles in Figure 2 comes from differences in production, rather than transport. In the right panel, which focuses on the TTL, a vertical line at the ozone concentration of the modern cold point tropopause (about 0.12 ppmv) is included to highlight where the cold point tropopause would be if it were to follow the same ozone concentration level as the troposphere expands.

212

4.2 Cold Point Tropopause Temperature and Water Vapor

213

214

215

216

217

218

Using the ozone profile shown in Figure 2 and the corresponding profile for JJA, temperature profiles were calculated for an idealized tropospheric expansion of 30 hPa. These are shown in Figure 3, with the modern temperature profile with and without a 30 hPa offset included for reference. The change in the height and temperature of the cold point tropopause for profiles with modified ozone relative to the shifted profiles is listed to emphasize the changes to the temperature structure of the TTL.

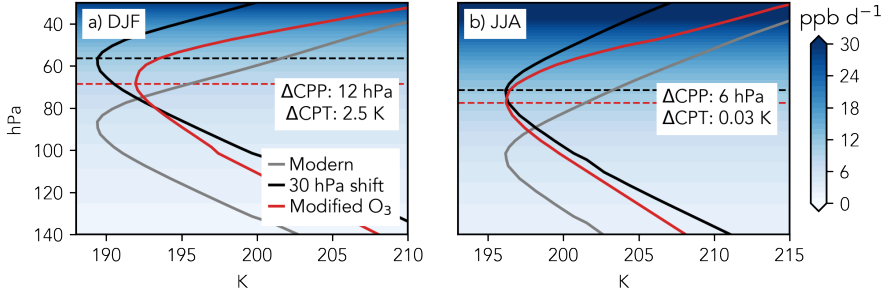


Figure 3. The upward shift of the cold point tropopause is limited in profiles that include ozone production (red) relative to those that are purely shifted upwards (black). Ozone production is shown in the blue shading, and the changes in cold point tropopause pressure and height relative to the “30 hPa shift” profiles are included to highlight the thermodynamic impact of this effect.

219

220

221

222

223

224

225

226

227

228

The temperature profiles in Figure 3 show that the upward shift of the cold point tropopause is limited by its movement up the ozone production gradient. In DJF, this compression is 40% of the 30 hPa expansion, while in JJA the effect is 20% of the rate tropospheric expansion. This decreases the extent of subadiabatic cooling between the top of the troposphere and the cold point tropopause, which combines with increased local radiative heating to increase the cold point tropopause temperature by 2.5 K in boreal winter and 0.03 K in boreal summer. Given that the cold point tropopause is at higher altitudes in DJF today, this difference between the seasons is not surprising – ozone production increases non-linearly with height, so tropospheric expansion will have a greater impact on local ozone production when the tropopause is higher to start with.

229

230

231

232

233

234

These increases in the cold point tropopause temperature and decreases in pressure increase the water vapor concentration at the cold point tropopause by 1.3 and 1.2 ppmv for the DJF and JJA “Modified O₃” temperature profiles relative to their respective “Modern” temperature profiles. These are significant increases relative to the modern annual mean lower stratospheric water vapor concentration of about 4 ppmv and would lead to an increase in water vapor throughout the stratosphere.

235

4.3 Effects of enhanced upwelling

236

237

238

239

240

241

242

In state-of-the art climate models, the Brewer-Dobson circulation – as quantified by the upward mass flux at 70 hPa – accelerates by 7 to 10% per degree of surface warming (Abalos et al., 2021), although this signal could be due to the upwelling profile following the tropopause upwards (Oberländer-Hayn et al., 2016). Enhanced upwelling would lessen the sharpening of the ozone gradient shown in Figure 2 by decreasing the transit time of air from its ozone-poor origin to the cold point tropopause, and it would increase dynamic cooling throughout the TTL, thereby decreasing the cold point tropopause

243 temperature. Both of these effects could negate the results discussed above, so the anal-
 244 ysis is repeated here with a range of vertical velocity accelerations to determine the ro-
 bustness of the production mechanism.

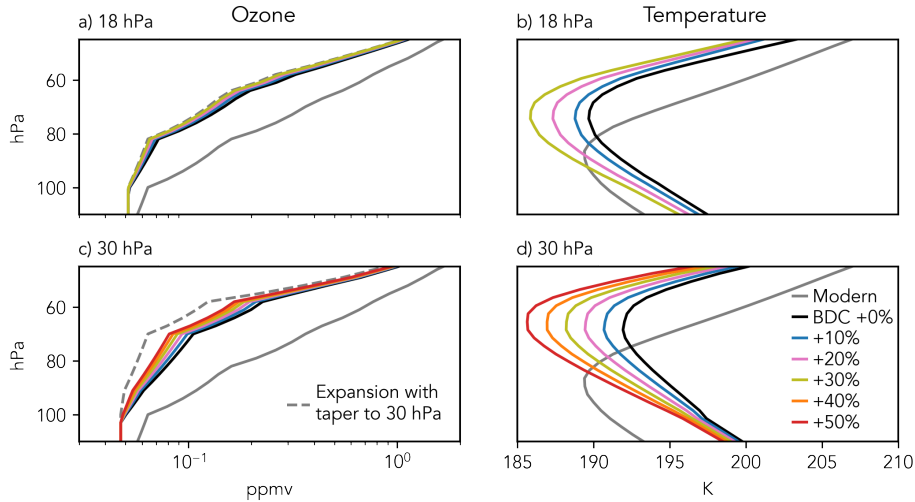


Figure 4. The effects of enhanced upwelling on lower stratospheric ozone (a and c) and temperature (b and d) profiles in DJF following 18 hPa (top row) and 30 hPa (bottom row) of tropospheric expansion. Details of the modified ozone profiles and radiative transfer calculations are described in the text, and corresponding profiles for JJA are shown in Figure S4.

245

246 To create ozone profiles that emulate enhanced upwelling in the TTL and lower strato-
 247 sphere, the method used in Section 4.1 is modified with shorter timesteps; i.e. the path
 248 of air to the cold point tropopause is assumed to be the same, but the ozone production
 249 at each location is reduced because the air traverses the levels more quickly. As shown
 250 in the left column of Figure 4, ozone concentrations throughout the TTL and lower strato-
 251 sphere decrease as the transit time to each level is decreased, which is consistent with
 252 recent work showing that stronger upwelling will advect ozone-poor air deeper into the
 253 stratosphere (Match & Gerber, 2022). For 18 hPa of tropospheric expansion, the increase
 254 in the ozone concentration at the cold point tropopause is small and is nearly eliminated
 255 by the increased rate of upwelling, while the effect of increased ozone production can-
 256 not be negated by enhanced upwelling following 30 hPa of expansion. In cold point-relative
 257 coordinates, lower stratospheric ozone increases when ozone production dominates over
 258 increased upwelling rates.

259 Temperature profiles were then calculated with these ozone profiles and dynamic
 260 cooling rates amplified in proportion to the increased upwelling rates. As shown in the
 261 right column of Figure 4, enhanced upwelling quickly dominates over the effect of increased
 262 ozone production following 18 hPa of tropospheric expansion, while the change in cold
 263 point tropopause temperature remains positive in DJF following 30 hPa of expansion
 264 when the acceleration is less than 30%. Given that all analysis done here includes a ver-
 265 tical shift of the upwelling profile, the upward flux at a fixed pressure level of 70 hPa re-
 266 quired to overcome the effect of increased ozone production on the cold point tropopause
 267 could be outside of the range of model projections.

268 5 Discussion and Summary

269 5.1 Implications for recent observations

270 The ozone budget analysis performed here presents a mechanism for lower strato-
 271 spheric ozone to increase following tropospheric expansion, which can help explain the
 272 persistence of lower stratospheric ozone concentrations in recent decades despite an ex-
 273 pected decrease (Thompson et al., 2021). This mechanism’s foundation is the strength
 274 of the ozone production gradient in the lower stratosphere: photochemical ozone pro-
 275 duction is insensitive to the height of the tropopause, so moving the tropopause and lower
 276 stratosphere up in altitude will push them into a region with a larger ozone source.

277 If the Brewer-Dobson circulation accelerated over the past two decades, then an
 278 increase in the ozone production rate in the tropical lower stratosphere may have com-
 279 pensated for the decreased transit time of air ascending from the troposphere and ex-
 280 tratropical lower stratosphere. This would have maintained the local balance of trans-
 281 port and production and held ozone concentrations constant when measured in tropopause-
 282 following coordinates. Given that changes in ozone production near the tropopause are
 283 small for small rates of tropospheric expansion in the current climate, the apparent bal-
 284 ancing of transport and production following surface warming suggests that the Brewer-
 285 Dobson circulation must not have accelerated significantly in the past two decades, agree-
 286 ing with previous literature (Fu et al., 2019; Diallo et al., 2021). It is also possible that
 287 upwelling rates may have also been shifted upwards by tropospheric expansion and have
 288 not strengthened relative to the tropopause (Oberländer-Hayn et al., 2016).

289 5.2 Implications for future projections

290 In a region where ozone concentrations are determined by the balance of produc-
 291 tion and the transport of ozone-poor air, different mechanisms can dominate depend-
 292 ing on the height of the tropopause and the strength of the Brewer-Dobson circulation.
 293 Match and Gerber (2022) showed that enhanced transport of ozone-poor air from the
 294 troposphere can decrease lower stratospheric ozone concentrations even when using tropopause-
 295 following coordinates. The work presented here does not refute those findings – if the
 296 effects of enhanced upwelling were to dominate over increased production rates, ozone
 297 concentrations above the tropical tropopause would decrease due to the decrease in ozone
 298 production as air ascends to the lower stratosphere. Changes to ozone production above
 299 the tropopause may be small in the near future, but as the troposphere continues to warm
 300 and the tropopause moves further up the ozone production gradient, TTL and lower strato-
 301 spheric ozone concentrations will increase when measured relative to the tropopause.

302 This leads ozone concentrations to act as a radiative cap on the upward excursion
 303 of the cold point tropopause: when the LZRH is shifted up by 30 hPa, the cold point
 304 tropopause only shifts up by 18 hPa in boreal winter and 24 hPa in boreal summer, thereby
 305 limiting the amount of subadiabatic cooling that can occur between the two levels. The
 306 compression of the layer between the LZRH and the cold point tropopause is consis-
 307 tent with the findings of Lin et al. (2017), who showed that the LZRH and lapse rate
 308 tropopause both rise more than the cold point tropopause in a model with sea surface
 309 temperatures increased by 4 K. That work also noted an increase in lower stratospheric
 310 ozone and temperature when using tropopause-following coordinates, which can be ex-
 311 plained by the shift of the tropopause up the ozone production gradient described here.

312 In this study, ozone production above the LZRH is shown to increase the cold point
 313 tropopause temperature by about 2.5 K in boreal winter and 0.03 K in boreal summer
 314 following 5 K of surface warming and 30 hPa of tropospheric expansion without an in-
 315 crease in upwelling velocity at the cold point tropopause. This will increase of water va-
 316 por concentrations of air entering the stratosphere by greater than 1 ppmv, which would
 317 result in a positive climate feedback with a radiative forcing of about 0.25 W m^{-2} (Solomon

et al., 2010). Additionally, this increase in stratospheric water vapor would increase the availability of hydrogen oxide radicals, which catalyze ozone destruction at low latitudes (Dvortsov & Solomon, 2001), and contribute to high latitude ozone destruction by allowing chlorine activation to occur at higher temperatures (Drdla & Müller, 2012).

Finally, this work highlights the need for high vertical resolution data for studies of TTL and lower stratospheric composition and thermodynamics. In both models and observations, tropopause-following coordinates cannot be used if tropospheric expansion cannot be resolved. Temperature and ozone measurements taken at constant heights will not reveal subtle shifts in the cold point tropopause, which would mask the mechanism presented here as the surface warms. This can lead to spurious trends in local temperature and ozone concentration and disagreement between models and observations with differing vertical grids.

6 Open Research

SWOOSH ozone data can be accessed through NOAA’s Chemical Sciences Laboratory (<https://cs1.noaa.gov/groups/cs18/swoosh/>), ERA5 temperature and wind data can be accessed through Copernicus Climate Change Service (<https://apps.ecmwf.int/data-catalogues/era5/?type=an&class=ea&stream=oper&expver=1>), and Radio Occultation data can be accessed through the ROM SAF Product Archive (<https://www.romsaf.org/product\archive.php>; registration required). WACCM ozone production rates for 2004 to 2009 were supplied by Marta Abalos by email (mabalosa@ucm.es). LAGRANTO trajectory data, future WACCM ozone production rates, and code to produce figures are available on Zenodo (<https://doi.org/10.5281/zenodo.8219306> (Bourguet, 2023)). The Python interface for RRTMG was supplied through Konrad, which is available at <https://github.com/atmtools/konrad/blob/main/README.md>.

Acknowledgments

Thanks to Marianna Linz and Aaron Match for helpful conversations and feedback.

References

- Abalos, M., Calvo, N., Benito-Barca, S., Garny, H., Hardiman, S. C., Lin, P., ... Yoshida, K. (2021). The brewer–dobson circulation in cmip6. *Atmospheric Chemistry and Physics*, *21*(17), 13571–13591. Retrieved from <https://acp.copernicus.org/articles/21/13571/2021/> doi: 10.5194/acp-21-13571-2021
- Abalos, M., Randel, W., Kinnison, D., & Serrano, E. (2013). Quantifying tracer transport in the tropical lower stratosphere using waccm. *Atmospheric Chemistry and Physics*, *13*(21), 10591–10607. doi: 10.5194/acp-13-10591-2013
- Abalos, M., Randel, W. J., Kinnison, D. E., & Garcia, R. R. (2017). Using the artificial tracer e90 to examine present and future utls tracer transport in waccm. *Journal of the Atmospheric Sciences*, *74*(10), 3383–3403. doi: 10.1175/JAS-D-17-0135.1
- Ball, W. T., Chiodo, G., Abalos, M., Alsing, J., & Stenke, A. (2020). Inconsistencies between chemistry–climate models and observed lower stratospheric ozone trends since 1998. *Atmospheric Chemistry and Physics*, *20*(16), 9737–9752. Retrieved from <https://acp.copernicus.org/articles/20/9737/2020/> doi: 10.5194/acp-20-9737-2020
- Birner, T., & Charlesworth, E. J. (2017). On the relative importance of radiative and dynamical heating for tropical tropopause temperatures. *Journal of Geophysical Research: Atmospheres*, *122*(13), 6782–6797. doi: 10.1002/2016JD026445

- 366 Bourguet, S. (2023, August). *The Impact of Ozone Production on Future Cold Point*
 367 *Tropopause Warming and Expansion*. Zenodo. Retrieved from [https://doi](https://doi.org/10.5281/zenodo.8219306)
 368 [.org/10.5281/zenodo.8219306](https://doi.org/10.5281/zenodo.8219306) doi: 10.5281/zenodo.8219306
- 369 Bourguet, S., & Linz, M. (2022). The impact of improved spatial and temporal res-
 370 lution of reanalysis data on lagrangian studies of the tropical tropopause
 371 layer. *Atmospheric Chemistry and Physics*, 22(20), 13325–13339. Re-
 372 trieved from <https://acp.copernicus.org/articles/22/13325/2022/>
 373 doi: 10.5194/acp-22-13325-2022
- 374 Brewer, A. W. (1949). Evidence for a world circulation provided by the measure-
 375 ments of helium and water vapour distribution in the stratosphere. *Quarterly*
 376 *Journal of the Royal Meteorological Society*, 75(326), 351–363. doi: 10.1002/qj
 377 .49707532603
- 378 Chiodo, G., Polvani, L. M., Marsh, D. R., Ball, W., Muthers, S., Stenke, A., . . . Tsi-
 379 garidis, K. (2018). The ozone response to quadrupled co2 concentrations. *J.*
 380 *Climate*, 31(10), 3893–3907. doi: 10.1175/JCLI-D-17-0492.1
- 381 Davis, S. M., Rosenlof, K. H., Hassler, B., Hurst, D. F., Read, W. G., Vömel, H., . . .
 382 Damadeo, R. (2016). The stratospheric water and ozone satellite homogenized
 383 (swoosh) database: a long-term database for climate studies. *Earth system*
 384 *science data*, 8(2), 461–490. doi: 10.5194/essd-8-461-2016
- 385 Diallo, M., Ern, M., & Ploeger, F. (2021). The advective brewer–dobson cir-
 386 culation in the era5 reanalysis: climatology, variability, and trends. *At-*
 387 *mospheric Chemistry and Physics*, 21(10), 7515–7544. Retrieved from
 388 <https://acp.copernicus.org/articles/21/7515/2021/> doi: 10.5194/
 389 acp-21-7515-2021
- 390 Drdla, K., & Müller, R. (2012). Temperature thresholds for chlorine activation
 391 and ozone loss in the polar stratosphere. *Annales Geophysicae*, 30(7), 1055–
 392 1073. Retrieved from [https://angeo.copernicus.org/articles/30/1055/](https://angeo.copernicus.org/articles/30/1055/2012/)
 393 2012/ doi: 10.5194/angeo-30-1055-2012
- 394 Dvortsov, V. L., & Solomon, S. (2001). Response of the stratospheric tempera-
 395 tures and ozone to past and future increases in stratospheric humidity. *Jour-*
 396 *nal of Geophysical Research: Atmospheres*, 106(D7), 7505–7514. doi: 10.1029/
 397 2000JD900637
- 398 Eyring, V., Shepherd, T. G., & Waugh, D. W. (Eds.). (2010). *SPARC CCMVal Re-*
 399 *port on the Evaluation of Chemistry-Climate Models* (Vol. No. 5; Tech. Rep.).
 400 SPARC. Retrieved from [http://www.sparc-climate.org/publications/](http://www.sparc-climate.org/publications/sparc-reports/)
 401 [sparc-reports/](http://www.sparc-climate.org/publications/sparc-reports/)
- 402 Fu, Q., Solomon, S., Pahlavan, H. A., & Lin, P. (2019, nov). Observed changes
 403 in brewer–dobson circulation for 1980–2018. *Environmental Research Letters*,
 404 14(11), 114026. Retrieved from [https://dx.doi.org/10.1088/1748-9326/](https://dx.doi.org/10.1088/1748-9326/ab4de7)
 405 [ab4de7](https://dx.doi.org/10.1088/1748-9326/ab4de7) doi: 10.1088/1748-9326/ab4de7
- 406 Gettelman, A., Birner, T., Eyring, V., Akiyoshi, H., Bekki, S., Brühl, C., . . . Tian,
 407 W. (2009). The tropical tropopause layer 1960–2100. *Atmospheric Chemistry*
 408 *and Physics*, 9(5), 1621–1637. Retrieved from [https://acp.copernicus.org/](https://acp.copernicus.org/articles/9/1621/2009/)
 409 [articles/9/1621/2009/](https://acp.copernicus.org/articles/9/1621/2009/) doi: 10.5194/acp-9-1621-2009
- 410 Gettelman, A., Hegglin, M. I., Son, S.-W., Kim, J., Fujiwara, M., Birner, T., . . .
 411 others (2010). Multimodel assessment of the upper troposphere and lower
 412 stratosphere: Tropics and global trends. *Journal of Geophysical Research:*
 413 *Atmospheres*, 115(D3). doi: 10.1029/2009JD013638
- 414 Gleisner, H., Lauritsen, K. B., Nielsen, J. K., & Syndergaard, S. (2020). Eval-
 415 uation of the 15-year rom saf monthly mean gps radio occultation climate
 416 data record. *Atmospheric Measurement Techniques*, 13(6), 3081–3098. doi:
 417 10.5194/amt-13-3081-2020
- 418 Grise, K. M., Thompson, D. W. J., & Birner, T. (2010). A global survey of static
 419 stability in the stratosphere and upper troposphere. *Journal of Climate*,
 420 23(9), 2275 - 2292. Retrieved from <https://journals.ametsoc.org/view/>

- 421 journals/clim/23/9/2009jcli3369.1.xml doi: [https://doi.org/10.1175/](https://doi.org/10.1175/2009JCLI3369.1)
 422 2009JCLI3369.1
- 423 Hersbach, H., Bell, B., Berrisford, P., Hirahara, S., Horányi, A., Muñoz-Sabater, J.,
 424 ... Thépaut, J.-N. (2020). The era5 global reanalysis. *Quarterly Journal*
 425 *of the Royal Meteorological Society*, 146(730), 1999–2049. Retrieved from
 426 <https://rmets.onlinelibrary.wiley.com/doi/abs/10.1002/qj.3803> doi:
 427 10.1002/qj.3803
- 428 Ho, S.-p., Hunt, D., Steiner, A. K., Mannucci, A. J., Kirchengast, G., Gleisner, H.,
 429 ... others (2012). Reproducibility of gps radio occultation data for climate
 430 monitoring: Profile-to-profile inter-comparison of champ climate records 2002
 431 to 2008 from six data centers. *Journal of Geophysical Research: Atmospheres*,
 432 117(D18). doi: 10.1029/2012JD017665
- 433 Jonsson, A. I., de Grandpré, J., Fomichev, V. I., McConnell, J. C., & Beagley,
 434 S. R. (2004). Doubled co2-induced cooling in the middle atmosphere:
 435 Photochemical analysis of the ozone radiative feedback. *Journal of Geo-*
 436 *physical Research: Atmospheres*, 109(D24). Retrieved from [https://](https://agupubs.onlinelibrary.wiley.com/doi/abs/10.1029/2004JD005093)
 437 agupubs.onlinelibrary.wiley.com/doi/abs/10.1029/2004JD005093 doi:
 438 <https://doi.org/10.1029/2004JD005093>
- 439 Keeble, J., Hassler, B., Banerjee, A., Checa-Garcia, R., Chiodo, G., Davis, S., ...
 440 others (2021). Evaluating stratospheric ozone and water vapour changes in
 441 cmip6 models from 1850 to 2100. *Atmospheric Chemistry and Physics*, 21(6),
 442 5015–5061. doi: 10.5194/acp-21-5015-2021
- 443 Kluft, L., Dacie, S., Buehler, S. A., Schmidt, H., & Stevens, B. (2019). Re-
 444 examining the first climate models: Climate sensitivity of a modern radiative–
 445 convective equilibrium model. *Journal of Climate*, 32(23), 8111–8125. doi:
 446 10.1175/JCLI-D-18-0774.1
- 447 Lin, P., Paynter, D., Ming, Y., & Ramaswamy, V. (2017). Changes of the tropical
 448 tropopause layer under global warming. *Journal of Climate*, 30(4), 1245–1258.
 449 doi: 10.1175/JCLI-D-16-0457.1
- 450 Match, A., & Fueglistaler, S. (2021). Large internal variability dominates over global
 451 warming signal in observed lower stratospheric qbo amplitude. *Journal of Cli-*
 452 *mate*, 34(24), 9823–9836. doi: 10.1175/JCLI-D-21-0270.1
- 453 Match, A., & Gerber, E. P. (2022). Tropospheric expansion under global warm-
 454 ing reduces tropical lower stratospheric ozone. *Geophysical Research Letters*,
 455 49(19), e2022GL099463. doi: 10.1029/2022GL099463
- 456 Ming, A., Hitchcock, P., & Haynes, P. (2016). The double peak in upwelling and
 457 heating in the tropical lower stratosphere. *Journal of the Atmospheric Sci-*
 458 *ences*, 73(5), 1889–1901. doi: 10.1175/JAS-D-15-0293.1
- 459 Mlawer, E. J., Taubman, S. J., Brown, P. D., Iacono, M. J., & Clough, S. A.
 460 (1997). Radiative transfer for inhomogeneous atmospheres: Rrtm, a vali-
 461 dated correlated-k model for the longwave. *Journal of Geophysical Research:*
 462 *Atmospheres*, 102(D14), 16663–16682. doi: 10.1029/97JD00237
- 463 Oberländer-Hayn, S., Gerber, E. P., Abalichin, J., Akiyoshi, H., Kerschbaumer,
 464 A., Kubin, A., ... Oman, L. D. (2016). Is the brewer-dobson circulation
 465 increasing or moving upward? *Geophysical Research Letters*, 43(4), 1772-
 466 1779. Retrieved from [https://agupubs.onlinelibrary.wiley.com/doi/abs/](https://agupubs.onlinelibrary.wiley.com/doi/abs/10.1002/2015GL067545)
 467 [10.1002/2015GL067545](https://agupubs.onlinelibrary.wiley.com/doi/abs/10.1002/2015GL067545) doi: 10.1002/2015GL067545
- 468 Perliski, L. M., Solomon, S., & London, J. (1989). On the interpretation of seasonal
 469 variations of stratospheric ozone. *Planetary and Space Science*, 37(12), 1527–
 470 1538. doi: 10.1016/0032-0633(89)90143-8
- 471 Randel, W. J., Park, M., Wu, F., & Livesey, N. (2007). A large annual cycle
 472 in ozone above the tropical tropopause linked to the brewer–dobson cir-
 473 culation. *Journal of the Atmospheric Sciences*, 64(12), 4479 - 4488. Re-
 474 trieved from [https://journals.ametsoc.org/view/journals/atasc/64/12/](https://journals.ametsoc.org/view/journals/atasc/64/12/2007jas2409.1.xml)
 475 [2007jas2409.1.xml](https://journals.ametsoc.org/view/journals/atasc/64/12/2007jas2409.1.xml) doi: 10.1175/2007JAS2409.1

- 476 Shepherd, T. G. (2008). Dynamics, stratospheric ozone, and climate change.
477 *Atmosphere-Ocean*, *46*(1), 117–138. doi: 10.3137/ao.460106
- 478 Solomon, S., Rosenlof, K. H., Portmann, R. W., Daniel, J. S., Davis, S. M., San-
479 ford, T. J., & Plattner, G.-K. (2010). Contributions of stratospheric water
480 vapor to decadal changes in the rate of global warming. *Science*, *327*(5970),
481 1219–1223. Retrieved from [https://www.science.org/doi/abs/10.1126/](https://www.science.org/doi/abs/10.1126/science.1182488)
482 [science.1182488](https://www.science.org/doi/abs/10.1126/science.1182488) doi: 10.1126/science.1182488
- 483 Sprenger, M., & Wernli, H. (2015). The lagranto lagrangian analysis tool – ver-
484 sion 2.0. *Geoscientific Model Development*, *8*(8), 2569–2586. Retrieved from
485 <https://gmd.copernicus.org/articles/8/2569/2015/> doi: 10.5194/gmd-8-
486 -2569-2015
- 487 Steiner, A., Hunt, D., Ho, S.-P., Kirchengast, G., Mannucci, A., Scherllin-Pirscher,
488 B., ... others (2013). Quantification of structural uncertainty in climate
489 data records from gps radio occultation. *Atmospheric Chemistry and Physics*,
490 *13*(3), 1469–1484. doi: 10.5194/acp-13-1469-2013
- 491 Thompson, A. M., Stauffer, R. M., Wargan, K., Witte, J. C., Kollonige, D. E.,
492 & Ziemke, J. R. (2021). Regional and seasonal trends in tropical ozone
493 from shadoz profiles: Reference for models and satellite products. *Journal*
494 *of Geophysical Research: Atmospheres*, *126*(22), e2021JD034691. Retrieved
495 from [https://agupubs.onlinelibrary.wiley.com/doi/abs/10.1029/](https://agupubs.onlinelibrary.wiley.com/doi/abs/10.1029/2021JD034691)
496 [2021JD034691](https://agupubs.onlinelibrary.wiley.com/doi/abs/10.1029/2021JD034691) (e2021JD034691 2021JD034691) doi: 10.1029/2021JD034691
- 497 Wild, O. (2007). Modelling the global tropospheric ozone budget: exploring the vari-
498 ability in current models. *Atmospheric Chemistry and Physics*, *7*(10), 2643–
499 2660. Retrieved from <https://acp.copernicus.org/articles/7/2643/2007/>
500 doi: 10.5194/acp-7-2643-2007